RSC Advances




ROYAL SOCIETY OF CHEMISTRY

www.rsc.org/advances

Journal Name

ARTICLE

# Oxygen Vacancies Dependent Au Nanoparticle Deposition and CO Oxidation

Received 00th January 20xx,
Accepted 00th January 20xx

DOI: 10.1039/x0xx00000x

www.rsc.org/

Xiuxiu Wang,[a] Beibei Chen,[a] Guozhu Chen,[b,*] and Xuan Sun[a,*]

Oxygen vacancy is critical for either the reactivity or the reaction mechanism for Au deposited oxide. Deposition behavior of Au on $CeO_2$ support was studied by mediating the content of oxygen vacancies by ascorbic acid (VC) treatment. Oxygen vacancies were introduced on $CeO_2$ nanorods (NRs) by VC reduction, and Au nanoparticles (NPs) were loaded by deposition-precipitation (DP) method. The formation of oxygen vacancies and its effects on the Au NPs deposition were evaluated by catalytic CO oxidation. The reaction mechanism of Au anchoring was closely linked to the concentration of oxygen vacancies. On the $CeO_2$ nanorods with optimal number of oxygen vacancies, deposition of Au behaviors more like a "lattice substitution mechanism", where charge transfer occurs to form positively charged $Au^{3+}$ species and reduced $Ce^{3+}$ associated with the creation of oxygen vacancies, which are active for CO oxidation. VC treatment induced large number of oxygen vacancies on $CeO_2$ NRs, resulting in highly increased reducibility of $CeO_2$ and strong interaction between Au and $CeO_2$. Consequently, $Au^{3+}$ cations were reduced directly with fast reduction rate instead of hydrolysis into hydroxychloro gold (III) complex $[Au(OH)_xCl_{4-x}]^-$ that was generally generated during the DP procedure. Such strong charge transfer interaction between the oxygen vacancies and $Au^{3+}$ leads to sintering of the reduced Au species to form Au NPs with bigger size and uneven distribution, and to decreased $Ce^{3+}/Ce^{4+}$ ratio with a decrement of surface oxygen atoms, as well as the reduction of $Au^{3+}$ species to $Au^{1+}$, which are altogether connected to the catalysis activity loss.

## Introduction

Ceria, a key component in the formulation of catalysts and catalyst supports, has received extensive investigation on various catalytic reactions. The high catalytic activity of $CeO_2$ originates from the rapid reduction/oxidation shift between $Ce^{3+}$ and $Ce^{4+}$, accompany with the formation and depletion of oxygen vacancies on the ceria surface or in the bulk, providing a high oxygen storage capacity (OSC), which is critical in determining the $O_2$ diffusion, the rate-controlling step in CO oxidation reaction.[1,2] The oxygen uptake and release relies on the rates of the redox cycles, where the oxidation of cerium is fast while reduction is sluggish. From this viewpoint, any processing on $CeO_2$ that favours the formation of oxygen vacancies will result in enhanced oxygen diffusion rate, giving rise to improvement of the catalytic activity of $CeO_2$. Qu *et al.*[3] used ascorbic acid (VC) and hydrogen peroxide to chemically etch the surface of ceria nanorods, which successfully in increase of the specific surface area, oxygen vacancies and surface $Ce^{3+}$ fractions with steadily increased CO oxidation reaction activity.

Additionally, $CeO_2$ has been recognized as a good reducible supports for Au nanoparticles (NPs) to perform as composite catalyst.[4] The key function of the support is to prevent abnormal growth of active Au particles, and the interaction between gold and the support is the determinant for catalytic activity. A synergic effect occurs between the gold particles and $CeO_2$ at the Au−$CeO_2$ interface, where redox processes are involved across oxygen vacancies, and allowing lattice oxygen atoms from the support to become activated species available for the oxidation reactions.[5,6] Theoretical studies have shown that the highly electro-negative Au NPs can bind strongly to the surface of $CeO_2$ enriched with oxygen vacancies. Oxygen vacancies may be the nucleation centres for the Au NPs, allowing the growth of small and well-dispersed Au clusters, which facilitate the reactivity of the catalyst.[7,8] Therefore, the presence of oxygen vacancies affects both the reactivity of the support and the gold dispersion on the material, modifying the electronic properties of the gold particles. When Au species bind on a highly reduced $CeO_2$ surface, electron transfer occurs between the $Ce^{3+}$, oxygen vacancy and the Au ions, leading to the variations in the Au charge. Identifying the chemical states of the active form of gold (i.e., metallic versus ionic) has still been the vigorous debate in literatures. The nature of the gold-oxygen vacancy interactions on $CeO_2$ surfaces have been studied by density functional theory calculations (DFT). If Au was absorbed on a surface $Ce^{3+}$ and subsurface oxygen atoms,

[a] *Key Laboratory of Colloid and Interface Chemistry, Ministry of Education, School of Chemistry and Chemical Engineering, Shandong University, Jinan 250100, P. R. China. E-mail: sunxuan@sdu.edu.cn; Fax: +86-531-88564464; Tel: +86-531-88362326*
[b] *School of Chemistry and Chemical Engineering, Jinan University, 250022, P. R. China*

† Electronic Supplementary Information (ESI) available: TEM images of the supporters and the Au-$CeO_2$ with their EDS, XRD pattern of the as-prepared samples. See DOI: 10.1039/x0xx00000x

Au will be negatively charged due to the transfer of the localized electron on $Ce^{3+}$ to the Au 6s orbital,[9,10] while the resulting $Au^{\delta-}$ is inert towards CO adsorption.[11,12] Using oxygen vacancy sites as the anchoring site for Au clusters, the Au in contact with surface O atoms is positively charged.[13,14] Fabris et al.[15] have suggested that the CO oxidation activity was associated with the chemical states of Au atoms at the interface. Specifically, $Au^{3+}$ ions dispersed into the ceria lattice as substitutional point defects could sustain a full catalytic cycle. Instead, the supported $Au^{+}$ atoms were readily attracted by oxygen vacancies to be turned into negatively charged $Au^{\delta-}$ species that deactivate the catalyst. Quite recently, Sheu[16] revealed that without oxygen vacancies, the Au atom adsorbed on a Ce vacancy of $CeO_2$(111) was highly positively charged. Increasing the number of oxygen vacancies lead to the decreased charge on Au from +3 to -1. Furthermore, with identical number of oxygen vacancies, the Au charge also relies heavily on the locations of the oxygen vacancies, suggesting the potential to adjust the oxidation states of Au atoms absorbed on ceria.

Experimentally, it is generally accepted that the structure and size of supported gold are greatly affected by nature and concentration of the oxygen vacancies coming from diverse preparation methods and reaction conditions. Nonetheless, relative little has been known on the properties of the deposited Au and Au-$CeO_2$ interaction by meditating the oxygen vacancies on the support. By modification of the redox properties of the support, the electronic interactions between the metal NPs and the support can be regulated in parallel. Weststrate et al.[17] initially studied the influence of oxygen vacancies on the properties of ceria-supported gold. They deposited Au by evaporation of Au metal on the oxidized and reduced $CeO_x$ substrates, respectively, and found that Au particles on the reduced $CeO_x$ with higher concentration of $Ce^{3+}$ were somewhat larger than on the oxidized substrate. Although they tried to disclose the charge state of Au in the same work, no explicit conclusion was obtained. Only, they demonstrated that small Au particles adsorbed on oxygen vacancies exhibit a significantly higher Au 4f binding energy than Au particles on oxidized $CeO_2$. With cation doping and substituting, oxygen vacancies can be populated in $CeO_2$,[18-21] which afterwards can be employed for the preparation of gold catalysts looking for small sizes of the gold NPs, and to meditate the properties of deposited Au.[21-24] By studying the influence of different dopants on the catalytic performance of nano-Au/$CeO_2$, Reddy et al.[25] found that incorporation of $Zr^{4+}$ into the Au/$CeO_2$ resulted in high CO oxidation activity attributed to the presence of more $Ce^{3+}$ ions and oxygen vacancies, which had a beneficial effect toward the gold dispersion, leading to smaller gold particles. Further, he disclosed that the presence of small Au particles is not the only prerequisite for achieving high CO conversion, the oxidation state of gold also plays a crucial role in the CO oxidation, and the metallic $Au^0$ was supposed to be the exclusive active species for CO oxidation at quite low temperatures. With the $Eu^{3+}$ doped $CeO_2$ support, Hernández et al.[26] demonstrated that the presence of higher concentration of oxygen vacancies induced by Eu-doping interact directly with gold during deposition-precipitation (DP), leading to smaller gold particle size with higher gold dispersion that can promote the reducibility of the catalysis. However, the overall activity of CO oxidation for Au/CeEu(10) was dropped compared with that of the Au/$CeO_2$. Unfortunately, they never disclosed the specific nature of such interaction from the point of charge transfer between Au and the support.

Meanwhile, it should be noticed that the oxygen vacancies are very important in determining the growth mechanism of the Au NPs. For the DP procedure, which is one of the mostly employed method to prepare active supported Au catalysts with aqueous $HAuCl_4$ as the gold precursor, it is generally recognized that the supported Au NPs are obtained from the insoluble $Au(OH)_3$ intermediate, which is hydrolysed from the adsorbed Au ions, usually the $AuCl_3$, and precipitation of $Au(OH)_3$ takes place exclusively on defects that act as nucleating sites.[27] Therefore, the nature of the solid surfaces is crucial in governing the formation of the Au NPs, and the surface with a high density of oxygen vacancies will lead to stabilized Au NPs of small size and narrow dispersion. Nevertheless, due to the complexity of the catalyst preparation process, the dependence of the initial nucleation and electronic structure of the supported Au nanoparticles on the structure of the support, specifically the oxygen vacancies, still remain unexplored. When the support with oxygen vacancies has a certain degree of reducibility, direct reduction of Au anions becomes possible. Questions arise: During DP procedure, which reaction pathway, direct reduction vs anions hydrolysis, is preferential? How does the reaction pathway affect the morphology, size and structure of the Au NPs? The influence of the oxygen vacancies on the reaction path and Au NP formation mechanism has been paid less attention, but is crucial in determining the metal–oxide interactions and the catalytic activity. Aiming at this doubt and to have a further insight into the electronic interactions occurring between the metal NPs and the support, in this work, we attempt to partially reduce $CeO_2$ and study the effect of oxygen vacancies on Au NPs deposition in DP procedure. Herein, ascorbic acid (VC) is employed since it is a well-known reducing reagent for Ce (IV). Previously, Qu *et al.*[3] found that redox cycles between $Ce^{3+}$ and $Ce^{4+}$ could be facilely implemented using $H_2O_2$ as oxidant and VC as reductant, respectively, which could be identified from the colour change and photoluminescence switch accordingly. Importantly, the nanorods morphology of the sample was well maintained during the VC reduction, which avoided the influence from the morphological and structural factors but disclosed a direct relationship between the electronic structure (valence state) and the physical properties (photoluminescence). Accordingly, it is expected that oxygen vacancies would be introduced along with the partial reduction of Ce (IV) in $CeO_2$ by VC treatment to afford a platform for investigating the deposition behaviour of the supported Au NPs. In the present work, the deposition behaviour of the Au NPs is comparatively studied between the VC treated $CeO_2$ NRs and pristine ones after DP. We found that VC treatment had a great effect on the introduction of oxygen

vacancy, and influences the Au NPs deposition behaviour as well as their catalytic activity toward CO oxidation.

## Experimental Section

### Materials

Cerium (III) nitrate hexahydrate ($Ce(NO_3)_3{\cdot}6H_2O$), sodium hydroxyl (NaOH), hydrogen tetrachloroaurate hydrate (auric acid, $HAuCl_4{\cdot}3H_2O$), and ammonium carbonate ($(NH_4)_2CO_3$), L-VC ($C_6H_8O_6$) are of analytical grade and are used without further purification.

### Preparation of $CeO_2$ NRs

The $CeO_2$ NRs were prepared by hydrothermal method as described by Yan's group.[28] Typically, $Ce(NO_3)_3{\cdot}6H_2O$ (0.05M) and NaOH (6M) were dissolved in 5 and 35 mL of deionized water, respectively. Then, these two solutions were mixed in a Teflon bottle, and this mixture was kept stirring for 30 min with the formation of a milky slurry. Subsequently, the Teflon bottle with this mixture was held in a stainless steel vessel autoclave, and the autoclave was sealed tightly. Finally, the sealed autoclave was then transferred to an oven at 100 °C, and held for 24 h. After hydrothermal reaction, the precipitates were filtered, washed with deionized water and dried at 60 °C under vacuum for 12 h.

### VC Treatment for $CeO_2$ NRs

120 mg of the as-prepared $CeO_2$ NRs were dispersed in 30 ml of water. Upon addition of 88 mg of VC, the mixture solution was stirred for 2h continuously at room temperature. Then the mixture was centrifuged and washed with deionized water and dried at 60 °C under vacuum for 12 h.

### Preparation of $CeO_2$ NR-Au catalysts

Pristine or VC treated $CeO_2$ NRs (150 mg) was dispersed in 7.5 ml of water whilst stirring and aqueous $(NH4)_2CO_3$ solution (3.75 ml; 1M) was then added. $HAuCl_4{\bullet}3H_2O$ (99.99%, Alfa; 0.0261 mmol) was dissolved in 3.75 ml of water and added to the above solution dropwise. The pH value was kept at 8-9 during the whole process. The resulting precipitate was aged at room temperature for 1 h, then filtered and washed three times with water. The product was dried in vacuum at 60 °C overnight and then calcined in air at 400 °C for 4h.

### Catalytic Oxidation for CO

Catalytic activity was measured using a continuous flow fixed-bed micro-reactor at atmospheric pressure. In a typical experiment, the system was first purged with high purity N2 gas and then a gas mixture of $CO/O_2/N_2$ (1:10:89) was introduced into the reactor which contained 50 mg of samples. Gas samples were analysed with an online infrared gas analyser (Gasboard-3121, China Wuhan Cubic Co.) which simultaneously detects CO and CO2 with a resolution of 10 ppm. The results were further confirmed with a Shimadzu Gas Chromatograph (GC-14C).

### Characterization

The samples were characterized by X-ray diffraction (XRD) on a Japan Rigaku D/Max-γA rotating anode X-ray diffractometer equipped with graphite-monochromatized Cu Kα radiation (λ=1.54178 Å) at a scanning rate of $0.02°{\cdot}s^{-1}$ in the 2θ range from 10° to 80°. The morphology and structure of samples were characterized by transmission electron microscopy (TEM, JEOL 6300, 100 kV) and high-resolution TEM (HRTEM, JEM-2100, 200 kV) equipped with energy-dispersive X-ray spectroscopy (EDS, Oxford INCA). X-ray photoelectron spectroscopy (XPS) spectra were recorded on an ESCALAB 250 spectrometer with a standard Al Kα source. The charging of the samples was corrected by referencing all of the energies to the C 1s peak energy set at 285.1 eV, arising from adventitious carbon. Optical absorption spectra were taken using a Varian 5000 spectrophotometer. Micro-Raman spectra were acquired with a RM 1000 Renishaw Raman Microscope System equipped with a laser at 633 nm.

## Results and Discussion

**Morphology and surface structure characterization.** The as-prepared **$CeO_2$ NRs** are reduced by VC in the first step (namely **VC-$CeO_2$**) to introduce oxygen vacancies, and then Au NPs are deposited on the oxygen vacancy sufficient surface by DP method to form the nanocomposite **Au/VC-$CeO_2$**. Controlled experiments are also carried out, where Au NPs deposited on pristine **$CeO_2$ NRs** by DP procedure are also obtained as **Au/$CeO_2$**.

Upon addition of VC into the pristine **$CeO_2$ NRs** slurry, colour changes rapidly from light yellow to deep brown, as shown by the insets in Figure 1a. The significant changes in colour may indicate the VC induced reduction on $CeO_2$, which can be verified by the changes in the UV-Vis spectra shown in Figure 1a. The pristine **$CeO_2$ NRs** present a typical intense absorption band with maximum at 310 nm, which is ascribed to the charge transfer absorption bands from oxygen to cerium.[5] The charge transfer from $O^{2-}$ to $Ce^{3+}$, and that from $O^{2-}$ to $Ce^{4+}$ cannot be clearly distinguished here. However, when adding VC, this absorption shifts to longer wavelength region, indicating the reduction of $Ce^{4+}$ to $Ce^{3+}$ since the electron transition from $O^{2-}$ to $Ce^{3+}$ is low-energy shift relative to that from $O^{2-}$ to $Ce^{4+}$. This transition from $Ce^{4+}$ to $Ce^{3+}$ will accompany with the formation of the oxygen vacancies due to a charge compensation mechanism.[29] Accordingly, the band gaps (BG) of the samples can be estimated by plotting the square root of the Kubelka-Munk function[30,31] multiplied by

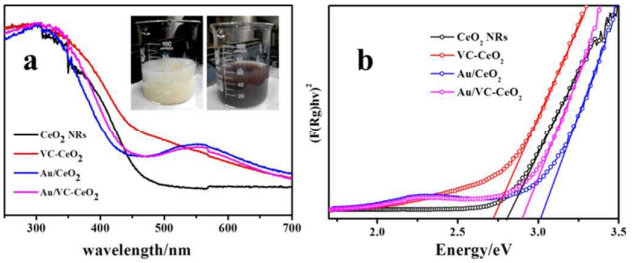


**Figure 1.** Electronic absorption of **$CeO_2$ NRs**, **VC-$CeO_2$**, **Au/$CeO_2$**, and **Au/VC-$CeO_2$**. Insets are the photographs of the slurry of **$CeO_2$ NRs** (yellow) and **VC-$CeO_2$** (brown), respectively.

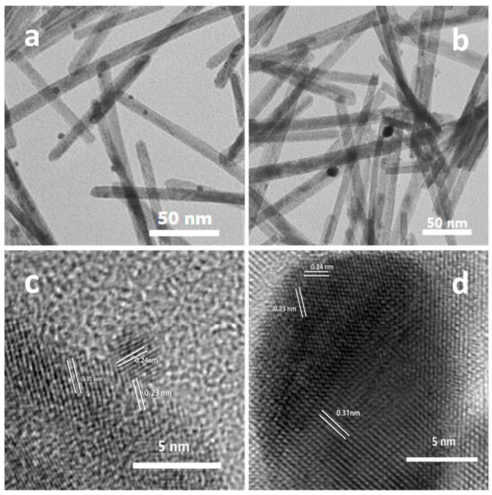


**Figure 2.** TEM images of (a) **Au/CeO$_2$**, (b) **Au/VC-CeO$_2$** and HRTEM identification of (c) **Au/CeO$_2$**, (d) **Au/VC-CeO$_2$**.

$(\alpha h\nu)^2$ versus photon energy ($h\nu$), and extrapolating linear part of the rising curve to zero (Figure 1b). It is found that on account of VC reduction, the BG decreased from 2.8 eV for pristine **CeO$_2$ NRs** to 2.7 eV for **VC-CeO$_2$**. It is worthy to mention that according to some recent studies on photocatalysis,[32] BG can be efficiently reduced by introduction of oxygen vacancy states between valence band and conductive band. Herein, the decrement of the BG may suggest the generation of oxygen vacancies associated with reduction.

After introduction of gold species, an additional broad absorption band centred at about 560 nm appears (in Figure 1a), which is ascribed to the surface plasmon (SP) resonance of Au nanoparticles as signature for the presence of metallic $Au^0$ nanoparticles.[5] The intensity of the SP band is slightly lowered for **Au/VC-CeO$_2$**, which may indicate a decreased Au content on the VC reduced support. Meanwhile, the absorption corresponding to the charge transfer transitions from O to Ce blue-shifted slightly. Accordingly, the BG of the Au supported samples both increased relative to that of the **CeO$_2$ NRs** supports, i.e. 3.0 eV for **Au/CeO$_2$**, and 2.9 eV for **Au/VC-CeO$_2$** (Figure 1b). The increased BG of the Au supported $CeO_2$ may indicative of the oxygen vacancies consuming, i.e., a strong interaction between gold and the **CeO$_2$ NRs**, and probably changes in the $Ce^{3+}/Ce^{4+}$ surface ratio. It was figured out that during the DP process, an individual Au atom can occupy an oxygen vacancy, acting as the nucleation site for the growth of a gold cluster.[26,33] The present result agreed well with Zepeda's[5] investigation on the loading effect of Au on $CeO_2$, where the author pointed out that BG changes upon Au deposition was caused by changes in the $Ce^{3+}/Ce^{4+}$ surface ratio due to the interaction with Au species. It is therefore expected that the VC reduction would have a great influence in regulating the metal-support interaction, and the redox properties of Au species and $CeO_2$, and consequently, the catalytic activity.

TEM and HRTEM (Figure 2) reveal the morphology of the VC treated $CeO_2$ NRs and those loaded with Au nanoparticles (NPs). As shown in Figure S1, the as-synthesized pristine **CeO$_2$ NRs** have a narrow diameter distribution in 8~10 nm and lengths of 100~400 nm, which is resemble to that of the Yan's work.[28] As expected, upon VC treatment, no distinctive changes can be observed in either the crystalline structure or surface morphology of **CeO$_2$** NRs though dramatic colour change was visualized (inset in Figure 1). This might also be an evidence for the reduction of $Ce^{4+}$ and formation of oxygen vacancies that contribute to the colour change.

After DP procedure, some dispersive dark sports are visualized for both the **CeO$_2$** NRs and **VC-CeO$_2$** (Figure 2a and 2b), which are speculated to be the deposited Au NPs. The Au particles highly dispersed on the surface of **CeO$_2$** NRs with small size of 3~5 nm. Compared with the pristine **CeO$_2$** NRs, the dark sports on the VC treated sample **VC-CeO$_2$** have the uneven distribution with the inhomogeneous size. The overall Au particle size grows up on the VC treated support (>5 nm), and some large Au particles with size of approximate 30 nm are observed, suggesting that VC treatment inducing agglomerates of the $Au(OH)_3$ precipitation during the DP procedure. The presence of the Au NPs can be evidenced from the lattice fringes in the HRTEM images (Figure 2c and 2d). After catalysed CO oxidation, the overall particle size of the Au deposited samples remain almost unchanged as visualized in TEM and HRTEM images (Figure S2), indicating the high stability of the samples under the present preparation conditions.

Other than the Au particle size and distribution, the loading capacity of the Au NPs is largely reduced from 0.5% for **Au/CeO$_2$** to 0.2% on the VC treated **CeO$_2$** as estimated from the EDS measurements, which is consist with the decreased intensity of the SP absorption in the electronic absorption spectra (Figure 1). The above results clearly indicate the VC treatment in intervening in the deposition behaviour of the Au NPs.

All the samples are also characterized by XRD measurement. The XRD patterns of pristine, VC treated $CeO_2$ NRs and their corresponding samples supported with Au NPs are given in Figure S3. Both pristine and VC treated $CeO_2$ NRs display similar diffraction patterns, indicating that the $CeO_2$ cubic fluoride crystal phase (JCPDS card No. 34-0394) is not changed upon VC treatment. Moreover, after the loading of Au, for either **Au/CeO$_2$** or **Au/VC-CeO$_2$**, there are no significant diffraction peaks indexed to Au, even the Au NPs can be clearly identified by HRTEM, implying that the Au particles were highly dispersed on the $CeO_2$ surface and/or low loading.[34,35]

**Reducibility evaluation.** $H_2$ temperature programmed reduction is carried out to characterize the reducibility of the $CeO_2$ NRs and the Au-containing catalysis in view of the structural discrepancy caused by VC treatment. Reduction patterns are depicted in Figure 3a and the temperatures of the peak maxima and their respective hydrogen consumption are summarized in Table 1. Both the pristine **CeO$_2$ NRs** and **VC-**



 

**$CeO_2$** show two main reduction peaks referring to the typical profiles of based ceria supports. The high temperature peak cantered around 800°C (HT peak) is due to bulk oxygen species, namely the total reduction of $Ce^{4+}$ to $Ce^{3+}$.[35-37] The exact HT peak position may relevant to the reducibility of the bulk material, which is correlated with the oxygen mobility as proposed by Hernández et al.[26] They found that the temperature of maximum HT peak of Eu-doped $CeO_2$, namely CeEu(10), was strongly decreased in comparison with the bare $CeO_2$ solid, which was ascribed to the presence of a high concentration of oxygen vacancies. For VC treated $CeO_2$ herein, the HT reduction peak shifts slightly toward low temperature, though marked colour changes are observed associated to $Ce^{4+}$ reduction. The broad peak at low temperature below 600°C (LT peak) is attributed to reduction of the oxygen vacancies including the surface oxygen species adsorbed on the vacancies. It is noteworthy that the shoulder at 385 °C is likely associated with reduction of the surface oxygen of $CeO_2$, while the peak at about 510 °C is due to the formation of nonstoichiometric Ce oxides, $CeO_x$ (x ranging from 1.9 to 1.7, or the β phase).[38] In Hernández's work,[26] it was suggested that Eu-doping induced increased concentration of oxygen defects in this solid. However, CeEu(10) demonstrated LT peaks at higher temperature than pure $CeO_2$. In contrast, no peak shift was observed for the VC treated $CeO_2$ in spite of the prompt reduction occurs in the bulk. However, the overall $H_2$ consumption reduced relatively after VC reduction. Actually, the $H_2$ consumption during the surface reduction step was related with the ability of the oxygen vacancies to adsorb and dissociate $H_2$.[17] From the lower $H_2$ consumption for **VC-$CeO_2$**, we speculate that VC reduction induced formation of $Ce^{3+}$ are mainly in $CeO_2$ lattice, while less for the formation of surface oxygen vacancies, which will be discussed hereinafter.

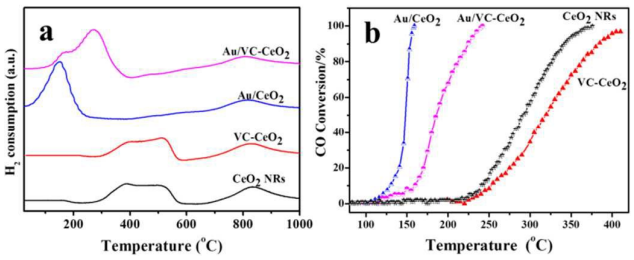


**Figure 3.** (a) $H_2$-TPR profiles and (b) CO conversion profiles of **$CeO_2$ NRs, VC-$CeO_2$, Au/$CeO_2$, and Au/VC-$CeO_2$.**

**Table 1.** TPR Peak Maxima and $H_2$ Consumption of **$CeO_2$ NRs, VC-$CeO_2$, Au/$CeO_2$, and Au/VC-$CeO_2$.**

| catalysts | Peak position (℃) | | $H_2$ consumption (*mmol/mg* of catalysts) | |
|---|---|---|---|---|
| | $T_{LT}$ | $T_{HT}$ | $\eta_{LT}$ | $\eta_{HT}$ |
| **$CeO_2$ NRs** | 385; 512 | 833 | 56.6 | 42.2 |
| **VC-$CeO_2$** | 386; 515 | 827 | 49.2 | 37.4 |
| **Au/$CeO_2$** | 149 | 817 | 125.5 | 48.2 |
| **Au/VC-$CeO_2$** | 160; 272 | 810 | 107.8 | 43.1 |

In the case of the reduction profiles of Au loaded catalysts, the HT peak shifts more than a dozen nanometers toward low temperature together with a little increased $H_2$ consumption compared with the respective supports, which may suggest a further improved oxygen mobility and reducibility within the bulk. While according to literatures,[33,35] the HT peak of the most reported gold/ceria catalysts remains unchanged upon Au deposition. We tentatively attribute the observed changes to be the indicative of the Au-$CeO_2$ interaction. In line with previous observations in literatures,[26,35,39] the most dramatic change upon Au addition is found in the low temperature region. The LT section shifts greatly to lower temperature accompany with highly increased $H_2$ consumption, as an indication of the increased surface oxygen reducibility. **Au/$CeO_2$** shows a single but slightly asymmetric peak centred at about 149°C, while the LT peak of **Au/VC-$CeO_2$** exhibits two overlapping reduction peaks at 160°C and 270°C, respectively. Such overlapped asymmetric LT peak on account of the Au deposition has ever been documented by Hernández et al.[26] for the Au/CeEu(10) catalysts. Compared with the single LT reduction peak of Au/$CeO_2$, peak splitting was observed for Au/CeEu(10) with higher concentration of oxygen vacancies. It was therefore deduced that the surface oxygen reducibility may related to interaction between the reducible species with the oxygen vacancies. However, the specific nature of this interaction was never specified in their work. According to the literatures concerning the chemical properties of Au species in the gold/ceria, the increased surface oxygen reducibility is denoted to the result of the pronounced Au–O–Ce interaction,[39] and it should be contributed from the reduction of both the surface ceria and the ionic gold species.[35] As documented previously,[33,35] this LT peak maxima and the $H_2$ uptake depend heavily on the reaction pathway of Au on ceria. In the case of the DP proceeded sample, a lattice substitution mechanism is proposed for the interactions between Au and support, namely, the ions $Au^+$ or $Au^{3+}$ would fill the vacant $Ce^{4+}$ sites with consequent formation of oxygen vacancies and increased oxygen mobility and reducibility. Herein, the $H_2$ reduction at low temperature region shows dramatically different behaviour for **Au/$CeO_2$** and **Au/VC-$CeO_2$**, suggesting the different interactions of Au with the pristine and VC treated ceria. Overall, the VC-treated samples, either the Au-free **$CeO_2$ NRs** or **Au/VC-$CeO_2$**, provide depressed reducibility as the consequence of the decreased surface oxygen vacancies.

Like the TPR process, the CO oxidation is also relying on the reducibility of the surface oxygen vacancies. Therefore as expected, VC treatment induces a negative effect on CO oxidation (Figure 3b). Specifically, both the Au-loaded samples exhibit remarkably higher activity than their corresponding $CeO_2$ support on account of the synergistic effect between the metal and support, which is in accordance with those related reports. However, **Au/VC-$CeO_2$** exhibits much tardier CO oxidation activity relative to that of **Au/$CeO_2$**. Even the $CeO_2$ support showed a little decreased reactivity upon VC reduction. Since VC can indeed reduce the $Ce^{4+}$ to $Ce^{3+}$, why does the VC-treatment induce a deactivation on CO oxidation? And how

does the VC-treatment influence the deposition behaviour of Au, as well as the interaction between Au and support? The key point is the oxygen vacancies. Therefore, the intimate correlation between the VC-reduction and the oxygen vacancies formation will be checked out hereafter. In fact, the same tendency of the reactivity for the $Au/CeO_2$ catalysis relying on the concentration of oxygen vacancies has been reported by Hernández et al.[26] The Au/CeEu(10) material being less active than the $Au/CeO_2$ despite having a similar gold particle size and structural and textural properties. Two principal possibilities were proposed to explain the lower activity: one was the loss of actives sites from the support (oxygen vacancies), the other was the possible electronic change induced on the gold particles. Both the two reasons involve the interactions between the metal and the support across the oxygen vacancies.

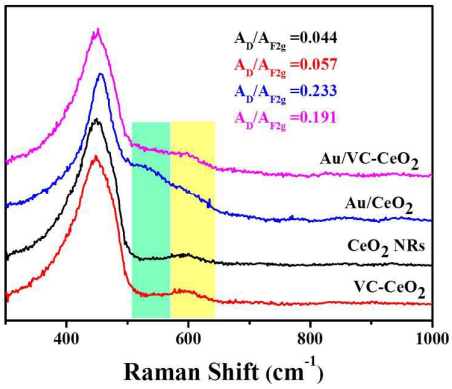


**Figure 4.** Raman spectra of **$CeO_2$ NRs**, **VC-$CeO_2$**, **$Au/CeO_2$**, and **Au/VC-$CeO_2$**.

**Oxygen vacancies and $Ce^{3+}$ influenced by VC treatment and Au deposition.** Raman spectroscopy is performed to study the electronic defects on the surface of nonstoichiometric $CeO_2$ in response to VC reduction and Au deposition. Figure 4 shows the visible Raman spectra of pristine, VC-treated $CeO_2$ NRs, and the corresponding Au-$CeO_2$ NRs samples. The Raman spectra of all samples are dominated by a strong absorption peak at 440~462 $cm^{-1}$, which is ascribed to the oxygen breathing vibrations ($F_{2g}$ mode) of fluorite-type structure of $CeO_2$.[26,40] The shift to lower frequency compared to the vibration at 466 $cm^{-1}$ from the **$CeO_2$** single crystal, and the broader and asymmetric character are attributed to the small particle size.[41] Both two $CeO_2$ supports, the original and the VC-treated ones, demonstrate almost identical characters within this energy region. In contrast, Laguna et al.[24] observed remarkable changes of this signal for Zr-doped ceria. They found the broadened and higher-energy shift of the $F_{2g}$ band along with increasing the Zr content, as the result of the particle size decrease and structural alteration by the inclusion of Zr into the cubic ceria lattice. It is therefore speculated that VC reduction induced little modification on the vibrational structure of $CeO_2$, as also indicated by the XRD results. One band at 600 $cm^{-1}$ (yellow stripe) is also observed, which is indexed to a defect-induced mode due to the presence of intrinsic oxygen vacancies generated by the partial reduction of $Ce^{4+}$ to $Ce^{3+}$.[42] By means of in situ Raman analysis, Vindigni et al.[41] proved that this peak was associated with the inner unreactive oxygen vacancies in water–gas shift (WGS) catalysts. The intensity of this band relative to that of $F_{2g}$, $I_{600}/I_{465}$, is generally the characterization of the number of the inner defects, which is increased after VC treatment compared to the pristine **$CeO_2$ NRs**, indicating the formation of incremental inner defects accompany with $Ce^{3+}$ ions. After loading of Au by DP method, the $F_{2g}$ peak shows clearly blue-shift compared with that of pristine **$CeO_2$ NRs**, which can be interpreted as a direct gold-support interaction across the oxygen vacancies. The blue-shift in $F_{2g}$ signal that indicates the electronic interaction between gold clusters and the support was also demonstrated in an Au loaded Ce-Zr catalysis.[24] Moreover, the most important is that by incorporation of Au, a new Raman absorption band at 540 $cm^{-1}$ (green stripe, D band) can be distinguished especially for **$Au/CeO_2$**. This band is typically observed in cation doped **$CeO_2$**,[26,42] which is attributed to the exogenous oxygen vacancy introduced by the substitution of tetravalent $Ce^{4+}$ with trivalent cations. This peak, which can be generated by hydrogen reduction and eroded upon re-exposure to $O_2$, manifests the presence of the reactive surface peroxides, $O_2^{2-}$.[43] For the VC-reduced $CeO_2$ NRs, the intensity of this band is strongly decreased when Au is deposited. Hernández et al.[26] have noticed the intensity variation of this band upon interact with doped Au. When Au deposited on Au/CeEu(10), the intensity of this band strongly decreased, almost disappearing. They referred such changes to a direct gold-support interaction across the oxygen vacancies by means of a "filling effect",[44] where the oxygen vacancies together with this vibrational mode eliminated as the result of the occupation of the oxygen vacancies by Au atoms. However, opposite results were demonstrated by Vindigni et al.[41] for the $Au/CeO_2$ catalysis. They found the presence of defects on AuCe673Ox that was evidenced by the appearance of this band, and attributed it to the synergic contribution of the highly dispersed gold that strongly interacting with the ceria surface. The formation of oxygen vacancies instead of elimination may denoted to a lattice substitution mechanism,[33] where ions $Au^+$ or $Au^{3+}$ would fill the vacant $Ce^{4+}$ sites with consequent formation of oxygen vacancies and increased oxygen mobility and reducibility.[35] Herein, the distinct diversity of the intensity of this band in **$Au/CeO_2$** and **Au/VC-$CeO_2$** may *crucially* reveal the discrepant reaction mechanism of Au species with the $CeO_2$ support. Overall, the variation of relative intensities of the peaks at 600 and 540 $cm^{-1}$ in Raman signals (listed in Table 2) may suggest that, first of all, VC treatment indeed reduced the $Ce^{4+}$ to $Ce^{3+}$ together with the formation of oxygen vacancies, which is dominantly associated to the inner defects, as evidenced by the markedly colour change shown in Figure 1a; secondly, deposition of gold by DP procedure leads to increment of oxygen vacancies, including both the intrinsic and the exogenous oxygen vacancies; the last but not least, compared with **$Au/CeO_2$**, when Au NPs deposited on the VC treated surface of $CeO_2$, it contributes less for the generation of the surface oxygen vacancies.

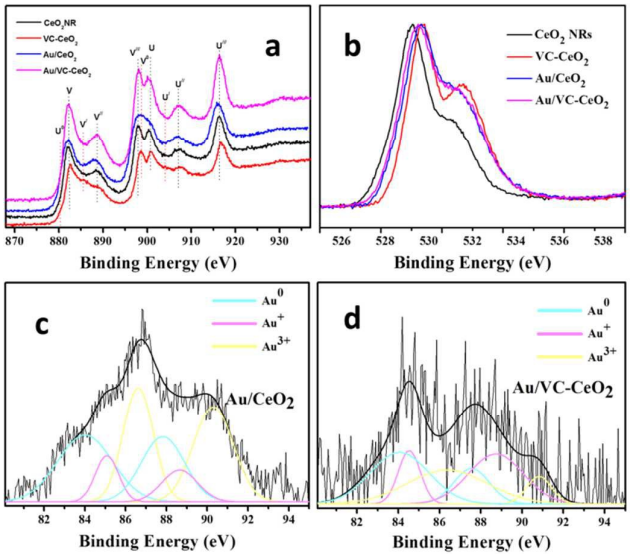


**Figure 5.** (a) XP spectra of the Ce 3d, (b) O 1s of **$CeO_2$ NRs**, **VC-$CeO_2$**, **Au/$CeO_2$**, and **Au/VC-$CeO_2$**, and Au 4f7/2 levels of (c) **Au/$CeO_2$**, and (d) **Au/VC-$CeO_2$**.

The above two diverse mechanisms, the "filling effect" and the "lattice substitution mechanism", are related with the Au-$CeO_2$ interaction that may leads to different properties of the metal and support, specifically the $Ce^{3+}/Ce^{4+}$ and $Au^0/Au^{\delta+}$ surface ratios, which are crucial in determining the reducibility. Information on the surface chemical states can be obtained from XP spectra as shown in Figure 5. The chemical states of Ce can be determined by analysing the Ce 3d spectra (Figure 4a), where peaks corresponding to Ce $3d_{5/2}$ and Ce $3d_{3/2}$ spin-orbit contributions are denoted as V and U, respectively. The peaks labelled $V^0$, $V^{/}$, $U^0$, and $U^{/}$ represent the Ce (III) state, and those labelled V, $V^{//}$, $V^{///}$, U, $U^{//}$ and $U^{///}$ are characteristic of Ce (IV) state.[5] The relative content of the $Ce^{3+}$ and $Ce^{4+}$ of all the samples obtained by calculating the relative integration areas under the curve of each deconvoluted peaks listed in Table 2. With regard to the VC treated $CeO_2$ NRs, **VC-$CeO_2$**, the intensity of the peaks belonging to Ce(III) increases compared with the pristine **$CeO_2$ NRs**, suggesting the increased content of Ce(III) ions created after VC treatment. The reduction of $Ce^{4+}$ and increment of $Ce^{3+}$ are as expected, which is associate with the band edge shift in the absorption spectra.

**Table 2.** Relative intensity of the peaks $I_{600}/I_{465}$ and $I_D/I_{F2g}$ indicative of the intrinsic and exogenous numbers of oxygen vacancies, respectively, and the [$Ce^{3+}$]% content of each sample in response to VC treatment and/or Au loading.

| Catalysts | [$Ce^{3+}$]/% | $I_{600}/I_{465}$ | $I_D/I_{F2g}$ |
|---|---|---|---|
| **$CeO_2$ NRs** | 25.88 | 0.089 | -- |
| **VC-$CeO_2$** | 30.39 | 0.104 | -- |
| **Au/$CeO_2$** | 33.81 | 0.222 | 0.380 |
| **Au/VC-$CeO_2$** | 30.10 | 0.165 | 0.190 |

When Ce(IV) is reduced to Ce(III), oxygen vacancies may arise to maintain the charge neutrality according to the following reaction mechanism:

$$2Ce^{4+}_{Lattice} + 4O^{2-}_{Lattice} \rightarrow V_o + O + 2Ce^{3+}_{Lattice} + 3O^{2-}_{Lattice}$$

Therefore, XPS studies concentrating on O species were also conducted. The O1s signal clearly shows two different surface oxygen species. The low binding energy peak ($O_\alpha$: 529-530 eV) is ascribed to lattice oxygen whereas the high binding energy peak ($O_ß$: 531-532.8 eV) is assigned to oxygen vacancies together with the surface adsorbed oxygen or surface hydroxyl species ($O_s$ + $OH_s$).[39] The peak area ratio of $O_ß$ to $O_\alpha$ (in Table S1) is checked to roughly assess the number of oxygen vacancies in these samples, from which it is apparently found that the concentration of the oxygen vacancies increased much as the result of the VC reduction. This increment, accompany with the increase of the $Ce^{3+}$, is mostly ascribed to the intrinsic oxygen vacancies as indicated by Raman analysis. After loading the Au particles by DP procedure, the proportion of $O_ß$ to $O_\alpha$ for **Au/$CeO_2$** increased compared with the support, indicating the formation of exogenous oxygen vacancies corresponding to the appearance of the D band in Raman spectra. **Au/VC-$CeO_2$**, on the contrary, demonstrates dramatically decreased $O_ß$ ratio relative to **VC-$CeO_2$**. Moreover, a notice should be paid on the changes of the $Ce^{3+}$ ratio upon Au loading. **Au/$CeO_2$** shows markedly increased $Ce^{3+}$ content comparing with the bare support. **Au/VC-$CeO_2$** demonstrates comparable $Ce^{3+}$ content to **VC-$CeO_2$** and the lower content than that of **Au/$CeO_2$** (as shown in Table 2). Considering the highly increased $Ce^{3+}$ number by VC reduction, such low $Ce^{3+}$ content in **Au/VC-$CeO_2$** may indicate a direct consumption of $Ce^{3+}$ by Au loading, which is on the contrary to the widely accepted mechanism that can promote the $Ce^{3+}$ generation. Here, we notice that a discrepancy is found between the XPS results and the absorption spectra in indication of the changes of $Ce^{3+}$ and the oxygen vacancies on account of Au deposition. It is reasonable since the band shift in absorption spectra in response to generation or consumption of $Ce^{3+}$ comes from the changes both in bulk and on surface, while XPS results mainly concern the changes on surface. Overall, the above results indicate that VC treatment on $CeO_2$ causes the reduction of $Ce^{4+}$ to $Ce^{3+}$ associated with the formation of oxygen vacancies. This reduction occurred both on the surface and in the bulk, resulting dominantly in the intrinsic oxygen vacancies. After then, when Au deposited on the pristine $CeO_2$ or **VC-$CeO_2$**, respectively, different reaction mechanisms are expected leading to the generation of either the intrinsic oxygen vacancies or the extrinsic ones as indicated by the Raman analysis.

Interactions between Au species and support can also be disclosed from changes of the oxidation states of Au species when deposited on surface of $CeO_2$. As shown in Figure 5c and 5d, Au species on the surface of either the pristine **$CeO_2$** or the VC treated on, carry different oxidation states of $Au^0$, $Au^+$, and $Au^{3+}$.[39] Comparing with **Au/$CeO_2$**, in **Au/VC-$CeO_2$**, the content of $Au^0$ is roughly the same, while the relative composition of $Au^+$ and $Au^{3+}$ changed a lot (Table S1). On the VC reduced surface, the amount of the $Au^{3+}$ decreased much and $Au^+$ becomes the dominate species. As disclosed previously,[39] for the water-gas shift reaction, metal nanoparticles ($Au^0$) do not

participate in the reaction. Non-metallic gold species ($Au^{+}$ and $Au^{3+}$) strongly associated with surface cerium-oxygen groups are responsible for the activity. For revealing the deactivation of $Au/CeO_2$ catalysts during the CO-PROX reaction, Zepeda et al.[5] found that activity loss was connected to the fast reduction of Au species and the changes in the redox properties of ceria. Accordingly, we speculate that in this case, the different catalytic activity of **$Au/CeO_2$** and **Au/VC-$CeO_2$** for CO oxidation also concerns mainly the $Au^{+}$ and $Au^{3+}$ instead of $Au^{0}$. By theoretical modelling, it is explored that the oxidation state of gold are related to CO adsorption energies, which is crucial in determining the catalytic reactivity. More electrons on Au, the weaker CO adsorption becomes. Therefore, the present experimental results provide direct evidence for the above theoretical speculation. Further evidence for the activity of $Au^{\delta+}$ in governing the CO oxidation can be found from the XPS analysis after the catalytic reaction (Figure S4). The $Au^{3+}$ for both two Au containing catalysis became almost depleted after reacting with CO. $Au^{+}$ in **Au/VC-$CeO_2$** was highly consumed in CO oxidation. On the other hand, metallic Au became the dominate species for both of the Au catalysis (Figure S4 and Table S2). These changes directly proved the participation of $Au^{\delta+}$ in catalytic oxidation, where $Au^{\delta+}$ ($Au^{3+}$ and $Au^{1+}$) are reduced to $Au^{0}$. Furthermore, it may speculated that $Au^{3+}$ is more superior than $Au^{1+}$ in oxidation since **$Au/CeO_2$** shows the much higher reducibility than **Au/VC-$CeO_2$** (Figure 3b). The activity of the Au species in CO oxidation is connected with the adsorption energy of CO which is beyond the scope of this study. Accompany with the changes of the oxidation states for Au species during CO oxidation, the exogenous oxygen vacancies were also diminished after oxidation reaction (as shown in Figure S5), which is suggested to be also the active component for CO oxidation. These findings clearly demonstrate the synergistic effect between the metal and support.

Herein, we would pay much attention to the diverse reaction mechanism of Au with $CeO_2$ supports as mention above. The discrepancy of the relative proportion of $Au^{+}$ and $Au^{3+}$ definitely indicate the different reaction mechanism of gold with **$Au/CeO_2$** and **Au/VC-$CeO_2$**. Density functional theory calculations (DFT) by Fabris *et al.*[15] revealed that the interaction between the Au atom and the stoichiometric $CeO_2$ surface involves a charge transfer from the adsorbate to the substrate, yielding a positively charged $Au^{\delta+}$ and reduction of a Ce ion; while binding of Au adatoms at oxygen vacancies of reduced surface entails strong rearrangement at the Au/oxide contact occurring from the reduced oxide surface to the supported metal atom, leading to partial oxidation of $Ce^{3+}$ to $Ce^{4+}$ and reduction of the Au species. In short, two reaction mechanisms for Au loaded on $CeO_2$ are proposed in previous investigations: “filling effect” and “lattice substitution mechanism”. These two mechanisms are actually adverse to each other and are still the open question for debate. It may simply define that in the former, Au interact with $Ce^{3+}$ (oxygen vacancies) to form metallic or negatively charged Au species as the result of the electron transfer from Ce to Au; for the latter, Au interact with $Ce^{4+}$ to form positively charged Au species associated with the generation of $Ce^{3+}$ (oxygen vacancies) due to the electron transfer from Au to Ce. Herein in our present study, we firstly demonstrate that both of the two reaction mechanisms may competitively concomitant, relying on the concentration of oxygen vacancies on the support surface.

On account of above XPS and Raman analysis, the dependence of the gold-supporting interaction on oxygen vacancies can be clearly found. The pristine **$CeO_2$ NRs**, bearing the optimal number of oxygen vacancies, will interact with Au by the lattice substitution mechanism, leading to the higher positively charged $Au^{3+}$ species together with increased amount of oxygen vacancies, which are beneficial for oxidation When Au particles deposited on the surface of **VC-$CeO_2$** with excess amount of oxygen vacancies, filling effect occurs, which induces the reduction of $Au^{3+}$ into $Au^{+}$ accompany with the oxidation of $Ce^{3+}$ to $Ce^{4+}$ and consequently the lost reactivity. Moreover, the size effect coming from different reaction mechanism should be considered. Highly dispersed Au nanoparticles with smaller size are obtained for **$Au/CeO_2$**. Instead, bigger sized Au NPs with lower loading amount are obtained for **Au/VC-$CeO_2$**. In agreement with our finding, Venezia et al.[35] have disclosed a spontaneous tendency of the gold to reduce its oxidation states by segregating out of the ceria lattice. Taking into account the fact that the size and distribution of Au NPs on surface of pristine and VC treated $CeO_2$ support are extremely discrepant, different reaction pathway of the Au species on $CeO_2$ supports may be expected with controlled amount of oxygen vacancies.

**Reaction pathway of Au on $CeO_2$ meditated by VC reduction.** During the VC treatment, the yellow color of **$CeO_2$ NRs**, originating from Ce(IV)-O(II) charge transfer, drastically changes to deep brown color due to the formation of nonstoichiometric structure ($CeO_{2-x}$), leading to the increment of defects in treated $CeO_2$ NRs. The relative intensity ratio of $I_{600}/I_{F2g}$ in Raman spectra discussed above provides direct evidence in support of increment of oxygen vacancy after treatment. However, after DP deposition of Au NPs, the changes of the oxygen vacancies display different trends, where the number of oxygen vacancies decreased sharply in **Au/VC-$CeO_2$** compared with **$Au/CeO_2$**, as observed in Raman and XPS spectra.

With regard to Au deposition by DP method, there is a well-established mechanism that a hydroxychlorogold (III) complex $[Au(OH)_xCl_{4-x}]^{-}$ is formed as the result of the consecutive exchange of $Cl^{-}$, coming from $HAuCl_4$, by $OH^{-}$ as the pH value increases during the DP process. However, kinetically, the exchange rate of the $Cl^{-}$ by $OH^{-}$ ligand on gold(III) complexes is sluggish. Therefore, when $HAuCl_4$ is mixed with VC-treated $CeO_2$ NRs that has high content of oxygen vacancies, there is a high possibility that Au ions would be reduced directly, instead of the formation of $[Au(OH)_xCl_{4-x}]^{-}$ complex. To verify this possibility, pristine and VC-treated $CeO_2$ NRs were dispersed in water respectively, and $HAuCl_4$ aqueous solution was added drop by drop. Interestingly, for VC-treated $CeO_2$ NRs, color changed into pink within few minutes; while for the pristine

one, one can hardly find any color change. After centrifugation and thoroughly washing, these two samples were further characterized by TEM (Figure S6). Spherical Au NPs are clearly observed supported on the VC-treated $CeO_2$ NRs (Figure S56). Instead, neither Au NPs nor Au signal in EDX spectrum is observed for the pristine $CeO_2$ NRs (Figure S6a). This result undoubtedly demonstrates the strong reducing ability of **VC-$CeO_2$** NRs, which can reduce Au ions to Au NPs quickly. In comparison to pristine **$CeO_2$ NRs**, the increased reducing ability of **VC-$CeO_2$** should come from the large number of generated oxygen vacancies. During the reduction procedure, **VC-$CeO_2$** with high content of oxygen vacancies transfers the electrons to Au ions, resulting in sharp decrease of oxygen vacancy, the oxidation of $Ce^{3+}$ to $Ce^{4+}$, together with the reduction of $Au^{3+}$ into $Au^{+}$ as demonstrated in XPS.

Overall, though VC is supposed to be a strong reductant to reduce the $CeO_2$ to generate higher number of oxygen species, the excess amount of oxygen species lead to several negative effects when loading Au by DP procedure, which are prejudice toward CO oxidation. The excess amount of oxygen species has strong reducing ability to reduce the $HAuCl_4$ promptly, resulting in Au NPs with large size; such strong electron transfer from oxygen species ($Ce^{3+}$) to $Au^{3+}$ induces increased number of $Au^{+}$. The $Au^{+}$ is inclined to diffuse into the vacancy and turns into negatively charged $Au^{\delta-}$ adspecies, which would inhibit the adsorption of molecular CO or $O_2$, leading to the deactivation of catalyst.[15] The decrease of oxygen species as the consequent of such strong charge transfer will also diminish the ability to weaken the C-O bond,[45] thus leading to the decrease of catalytic activity.

## Conclusions

VC treatment induces the reduction of $Ce^{4+}$ to $Ce^{3+}$ to and creation of oxygen vacancies in $CeO_2$ NRs, which are dominantly intrinsic oxygen vacancies that are inactive for CO oxidation. However, these increased oxygen vacancies endow the VC-treated $CeO_2$ NRs with a certain reduction ability, which can reduce $AuCl^{4-}$ ions to Au NPs directly instead of the formation of hydroxychlorogold(III) complex $[Au(OH)_xCl_{4-x}]^-$. Such reaction pathway, accompany with strong charge transfer between the Au species and oxygen vacancies on $CeO_2$, results in fast growth of Au NPs with large size. Meanwhile, the $Ce^{3+}$ generated by VC reduction is oxidized by $Au^{3+}$, leading to decreased $Ce^{3+}$ content, decrement of surface oxygen vacancies, and reduction of $Au^{3+}$ to $Au^{+}$. As a consequence, the overall CO oxidation is deactivated. This work proves that the Au deposition during DP procedure is strongly relying on the content of oxygen vacancies in $CeO_2$, while the charge transfer between the Au species and oxygen vacancies has double-edged effects on catalytic activity. On one hand, oxygen vacancies are binding site for Au atom to form highly dispersed small Au NPS. Charge transfer between Au and support induces positively charged $Au^{3+}$ species and $Ce^{3+}$ associated with the generation of oxygen vacancies. “Synergic effect” occurs at the gold−support interface, which can active the lattice oxygen atoms from the support to surface for the oxidation reactions. On the other hand, excess amount of oxygen vacancies induce strong reducing ability and strong charge transfer from support to Au, leading to agglomerated Au NPs and fast reduction of $Au^{3+}$ reactive species, therefore resulting in catalysis deactivation. Moreover, this work demonstrates that high degree of oxygen vacancies changes the Au NP formation pathway during the DP procedure, which may bring some enlightenment for the preparation of reducible metal oxides supported Au composite catalyst.

## Acknowledgements

The authors acknowledge financial support from the National Natural Science Foundation of China (21371109) and the ‘‘Taishan Scholar’’ project of Shandong Province. Ke Tang is acknowledged for his help with $H_2$-TPR measurements.

## Notes and references

‡ Footnotes relating to the main text should appear here. These might include comments relevant to but not central to the matter under discussion, limited experimental and spectral data, and crystallographic data.

1 D. R. Mullins, S. H. Overbury and D. R. Huntley, *Surf. Sci.*, 1998, **409**, 307.
2 L. J. Wu, H. J. Wiesmann, A. R. Moodenbaugh, R. F. Klie, Y. M. Zhu, D. O. Welch and M. Suenaga, *Phys. Rev. B*, 2004, **69**, 125415.
3 W. Gao, Z. Zhang, J. Li, Y. Ma and Y. Qu, *Nanoscale*, 2015, **7**, 11686
4 C. J. Zhang, A. Michaelides and S. J. Jenkins, *Phys. Chem. Chem. Phys.*, 2011, **13**, 22
5 J. A. Hernández, S. A. Gómez, T. A. Zepeda, J. C. Fierro-González and G. A. Fuentes, *ACS Catal.*, 2015, **5**, 4003.
6 F. F. Zhu, G. Z. Chen, S. X. Sun and X. Sun, *J. Mater. Chem. A*, 2013, **1**, 288.
7 E. Wahlström, N. Lopez, R. Schaub, P. Thostrup, A. Rønnau, C. Africh, E. Lægsgaard, J. K. Nørskov and F. Besenbacher, *Phys. Rev. Lett.*, 2003, **90**, 026101.
8 C. Zhang, A. Michaelides, D. A. King and S. J. Jenkins, *J. Phys. Chem. C*, 2009, **113**, 6411.
9 K. Kośmider, V. Brázdová, M. V. Ganduglia-Pirovano and R. Pérez, *J. Phys. Chem. C*, 2016, **120**, 927.
10 J.-F. Jerratsch, X. Shao, N. Nilius, H.-J. Freund, C. Popa, M. V. Ganduglia-Pirovano, A. M. Burow and J. Sauer, *Phys. Rev. Lett.*, 2011, **106**, 246801.
11 W. Song and E. J. M. Hensen, *J. Phys. Chem. C*, 2013, **117**, 7721.
12 P. Ghosh, M. Farnesi Camellone and S. Fabris, *J. Phys. Chem. Lett.*, 2013, **4**, 2256.
13 Z.-P. Liu, S. J. Jenkins and D. A. King, *Phys. Rev. Lett.*, 2005, **94**, 196102.
14 C. Zhang, A. Michaelides, D. A. King and S. J. Jenkins, *J. Am. Chem. Soc.*, 2010, **132**, 2175.
15 M. F. Camellone and S. Fabris, *J. Am. Chem. Soc.*, 2009, **131**, 10473.
16 M.-W. Chang and W.-S. Sheu, *Phys.Chem.Chem.Phys.*, 2016, **18**, 15884.
17 C. J. Weststrate, R. Westerström, E. Lundgren, A. Mikkelsen, and J.N. Andersen, *J. Phys. Chem. C,* 2009, **113**, 724.
18 W. Y. Hernández, M. A. Centeno, F. Romero-Sarria, and J. A. Odriozola, *J. Phys. Chem. C* 2009, **113**, 5629.

19 E. d. O. Jardim, S. Rico-Francés, F. Coloma, E. V. Ramos-Fernández, J. Silvestre-Albero, A. Sepúlveda-Escribano, *Appl. Catal. A: Gen.* 2014, **487**, 119.
20 O. H. Laguna, F. Romero Sarria, M. A. Centeno, J. A. Odriozola, *J. Catal.* 2010, **276**, 360.
21 T. R. Reina, S. Ivanova, M. I. Domínguez, M. A. Centeno, J. A. Odriozola, *Appl. Catal. A: Gen.* 2012, **419–420**, 58.
22 T. R. Reina, E. Papadopoulou, S. Palma, S. Ivanova, M. A. Centeno, T. Ioannides, J. A. Odriozola, *Appl. Catal. B: Environ.* 2014, **150–151**, 554.
23 T. R. Reina, W. Xu, S. Ivanova, M. Á. Centeno, J. Hanson, J. A. Rodriguez, J. A. Odriozola, *Catal. Today* 2013, **205**, 41.
24 O. H. Laguna, A. Pérez, M. A. Centeno, J. A. Odriozola, *Appl. Catal. B: Environ.* 2015, **176–177**, 385.
25 P. Sudarsanam , B. Mallesham, P. S. Reddy, D. Großmann, W. Grünert, B. M. Reddy, *Appl. Catal. B: Environ.*, 2014, **144**, 900.
26 W. Y. Hernández, F. Romero-Sarria, M. A. Centeno, J. A. Odriozola, *J. Phys. Chem. C* 2010, **114**, 10857.
27 A. Corma and H. Garcia, *Chem. Soc. Rev.*, 2008, **37**, 2096.
28 H. X. Mai, L. D. Sun, Y. W. Zhang, R. Si, W. Feng, H. P. Zhang, H. C. Liu, and C. H. Yan, *J. Phys. Chem. B*, 2005, **109**, 24380.
29 J. Wang, D. N. Tafen, J. P. Lewis, Z. L. Hong, A. Manivannan, M. J. Zhi, M. Li and N. Q. Wu, *J. Am. Chem. Soc.*, 2009, **131**, 12290.
30 J. Ng, S. Xu, X. Zhang, H. Y. Yang and D. D. Sun, *Adv. Funct. Mater.*, 2010, **20**, 4287.
31 N. Serpone, D. Lawless, R. Khairutdinov, *J. Phys. Chem.*, 1995, **99**, 16646.
32 J. Gan, X. Lu, J. Wu, S. Xie, T. Zhai, M. Yu, Z. Zhang, Y. Mao, S. C. I. Wang, Y. Shen, Y. Tong, *Sci Rep.* 2013, **3**, 1021.
33 Q. Fu, H. Saltsburg and M. Flytzani-Stephanopoulos, *Science*, 2003, **301**, 935.
34 H. Zhang, Y. Xie, Z. Sun, R. Tao, C. Huang, Y. Zhao, and Z. Liu, *Langmuir*, 2011, **27**, 1152.
35 A. M. Venezia, G. Pantaleo, A. Longo, G. Di Carlo, M. Casaletto, F. L. Liotta, G. Deganello, *J. Phys. Chem. B* 2005, **109**, 2821.
36 H.C. Yao and Y. F. Yu Yao, *J. Catal.*, 1984, **86**, 254.
37 S.-Y. Lai, Y. Qiu, S. Wang, *J. Catal.* 2006, **237**, 303.
38 J. Z. Shyu, W. H. Weber and H. S. Gandhi, *J. Phys. Chem.*, 1988, **92**, 4964.
39 S, Zhang, X. S. Li, B. B. Chen, X. B. Zhu, C. Shi and A. M. Zhu, *ACS Catal.*, 2014, **4**, 3481.
40 V. G. Keramidas and W. B. White, *J. Chem. Phys.*, 1973, **59**, 1561.
41 F. Vindigni, M. Manzoli, A. Damin, T. Tabakova and A. Zecchina, *Chem. Eur. J.*, 2011, **17**, 4356.
42 A. D. Liyanage, , S. D. Perera, , K. Tan, , Y. Chabal, and K. J. Balkus, *ACS Catal.*, 2014, **4**, 577.
43 V. V. Pushkarev, V. I. Kovalchuk, and J. L. d'Itri, *J. Phys. Chem. B*, 2004, **108**, 5341.
44 M. G. Sanchez, J. L. Gazquez, *J. Catal.* 1987, **104**, 120.
45 L.-S. Zhong, J.-S. Hu, A.-M. Cao, Q. Liu, W.-G. Song and L.-J. Wan, *Chem. Mater.*, 2007, **19**, 1648.

**Graphical Abstract**

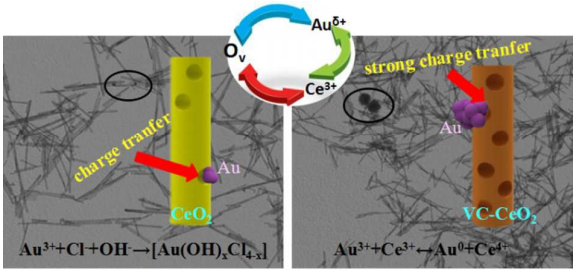


Au deposition pathway depends heavily on the oxygen vacancies numbers on $CeO_2$ support. With optimized oxygen vacancies, a "synergic effect" occurs between the gold particles and $CeO_2$ to promote the CO oxidation activity; excess oxygen vacancies lead to agglomerated Au NPs and reduction of $Au^{3+}$ reactive species with catalysis deactivation.